12.264

NEXRAD CORRECTION OF VERTICALLY INTEGRATED LIQUID IN AREAS OF PARTIAL BEAM BLOCKAGE

Kenta T. Hood*, Evelyn N. Mann, Betty J. Bennett, David J. Smalley
MIT Lincoln Laboratory, Lexington, Massachusetts

Pengfei Zhang
CIMMS, University of Oklahoma, and
NOAA/OAR National Severe Storms Laboratory, Norman, Oklahoma

Dusan Zrnic
NOAA/OAR National Severe Storms Laboratory, Norman, Oklahoma

1. INTRODUCTION

The safe and efficient routing of air traffic within the national airspace is a complex task that is further complicated when severe weather is present. The FAA is able to assess the severity of weather for proper route management through various weather observation systems that have been developed such as the Integrated Terminal Weather System (ITWS) (Evans and Ducot, 1994) and the Corridor Integrated Weather System (CIWS) (Evans and Ducot, 2006). A key product in these weather systems is Vertically Integrated Liquid (VIL) from NEXRAD.

Liquid water content (LWC) is the basis for VIL and is derived from reflectivity for each tilt. The VIL product is the integration of reflectivity-derived LWC over a column of space within a radar volume (Greene and Clark, 1972). It gives a three-dimensional depiction of storm structure in an easy-to-display two-dimensional product. A potential drawback to VIL is that the relation between LWC and reflectivity assumes a liquid state throughout the entire radar volume, even in subfreezing conditions. However, the ability to depict the structure of the atmosphere in three dimensions outweighs this drawback. To account for differences of lower and higher VIL levels between winter and summer, respectively, CIWS uses a winter precipitation scale for display to maintain winter structure detail.

A legacy VIL product has been available from NEXRAD as a low resolution Cartesian grid with 16 intensity levels at a spatial resolution of 4 km out to 230 km. Smalley and Bennett (2002) developed a higher resolution VIL product with 1° by 1 km resolution in polar form with coverage out to 460 km and 254 data levels. These additional capabilities of high resolution VIL provide the ability to monitor upwind convection and made it a candidate as a replacement for legacy VIL in FAA weather systems. This high resolution VIL product is now ingested by the critical FAA weather systems to create a mosaic over the CONUS for controllers to understand the state of the atmosphere.

The higher resolution VIL product was a step in the right direction but its quality is directly tied to the quality of reflectivity. The quality of reflectivity is most affected by contamination, partial beam blockage (PBB), and radar miscalibration. This paper notes advances dealing with contamination issues and explains PBB mitigation methods. Refer to Williams *et al.*, (2013) for a discussion on radar calibration.

Contamination of reflectivity data degrades the quality of the product. One source of contamination, ground clutter during anomalous propagation, would be manifest in areas outside the clutter map where clutter filters would not be

---

* *Corresponding Author Address*: Kenta T. Hood, MIT Lincoln Laboratory, 244 Wood Street, Lexington, MA 02420; e-mail: kenta.hood@ll.mit.edu

This work was sponsored by the Federal Aviation Administration (FAA) under Air Force Contract FA8721-05-C-0002. Opinions, interpretations, conclusions, and recommendations are those of the author and are not necessarily endorsed by the United States Government.

applied. Constant power contamination was also a problem and was manifested in the reflectivity data as a bull's-eye or sun strobe. To address these issues, a data quality assurance (DQA) algorithm was developed to remove contamination not accounted for in the upstream processing (Smalley *et al.*, 2003). Since then, additional DQA modules to remove sun strobes, spikes, and speckle have been added.

Another data quality issue in reflectivity data is PBB. In mountainous areas of the CONUS, reflectivity at lower elevation angle scans can be negatively biased due to this blockage. This bias affects the proper, full-volume computation of VIL and could cause potential safety issues when routing air traffic. The Denver and Los Angeles airports are examples of locations that could be negatively affected by blockage in the lower elevation scans. According to the 2011 FAA passenger boarding and all-cargo data, the Denver and Los Angeles airports were the 3rd and 5th busiest airports in the United States (FAA, 2013), respectively. Both radar locations experience beam blockage due to natural terrain. Some of the blockage is somewhat mitigated in the CIWS radar mosaic by having multiple radar sites in strategic, adjacent locations to cover areas of precipitation in the blocked areas. However, building more radar systems to cover areas of PBB is not an economically feasible option. An inexpensive solution would be to recover information in partially blocked areas with algorithms to correct for blockage.

A radar mosaic does not completely mitigate beam blockage. Beam blockage artifacts make their way into the CIWS VIL mosaic in a couple of ways. In areas where there is only one near range radar, if that radar is affected by PBB, the VIL from the beam blocked radar can be under-represented in the CIWS mosaic display resulting in precipitation intensity being too low. Figure 1 shows an example where the KABX (Albuquerque, NM) radar is affected by PBB where the only data available for the mosaic are from KABX.

The other beam blockage artifact in CIWS is due to the maximum plausible logic used to mosaic VIL data. In the CIWS system, each radar is flagged for areas of expected beam blockage by coupling terrain information with the radar location and lowest elevation in the scan strategy. The CIWS maximum plausible mosaic strategy for VIL attempts to use the highest plausible VIL value of any radar within near range, which is set to 230 km for NEXRAD. However, if there are no near range radars that are free of blockage, the highest VIL value overall from any radar with coverage of the area is used. The CIWS VIL mosaic can show discontinuities when data are not necessarily considered from nearby radars that are flagged as possibly being beam blocked and the mosaic switches to data from further away radars. An example of this type of artifact is shown in Figure 2.

In 2013, the upgrade of the NEXRAD WSR-88D weather radar network to dual polarization was completed. With the upgrade, additional data measurements and products are available for use in existing and future algorithms to improve the data quality of products. One of the new data measurements, differential phase (Φ_{DP}), is more immune to partial blockage of the beam and radar miscalibration than reflectivity. The National Severe Storms Laboratory (NSSL) has developed a new algorithm that uses a combination of differential phase and reflectivity to compute the specific attenuation along a radial (Zhang *et al.*, 2013). This specific attenuation term can be used to directly compute LWC to obtain a more accurate estimate of VIL.

This paper will discuss the current method used within the NEXRAD Open Radar Product Generator (ORPG) to correct for PBB. A basic description of the new algorithm to correct for PBB will be given followed by preliminary results.

2. BACKGROUND

2.1 Examples of Blockage

Under ideal conditions, a radar system will have unimpeded line of sight for maximal coverage to long range. However, partial or

complete blockage of the beam at various elevation angles occurs due to natural terrain (mountains, hills, trees, etc.) or man-made objects (buildings, radio towers, wind turbines). Anomalous propagation of the beam can make some blockage intermittent. Under these conditions, urban development can introduce blockage not once a concern.

An MIT Lincoln Laboratory analysis tool written in MATLAB allows visualization of blockage sources within Google Earth™. Examples of natural blockage to varying degrees due to mountainous terrain are shown in Figures 3 and 4. In Figure 3, Mt. Shasta partially blocks the 0.5° beam from the Medford, Oregon NEXRAD (located in reader's position out-of-page). The 147° radial at the left of the image is in an area of no blockage, the 148° radial has minimal blockage, and the 150° radial is almost completely blocked. Figure 4 shows a mountain range to the east of the Tucson, Arizona NEXRAD (located beyond right side of page). In the image, the radials extend out in range from right to left. Lower percentages of blockage can be seen as the beam begins to intersect the mountain. The blockage increases as the beam travels in range until it is completely blocked in some radials.

An example of man-made blockage can be seen in Figure 5 from the KOUN research radar in Norman, Oklahoma (located beyond lower left of image). Various structures on the campus of the University of Oklahoma can be seen to impinge the beam. Sarkey's Energy Center on the left of the image, the water tower, and Owen Field are all tall enough to partially block the beam. Man-made structures may not be accounted for in blockage maps and even if the structures are accounted for, when anomalous propagation occurs, the blockages increase while the algorithm assumes the lesser blockage percentages under standard propagation conditions.

To ensure adequate coverage overlap between radars at long ranges, the lowest elevation angles are most effective when free from blockage as much as possible. Over the entire NEXRAD network, just over a third of the radars (58 of 160) have a minimum of 50% blockage in at least 10% of the radials at the lowest elevation tilt. Most of these radars have more than 10% of the radials blocked, with some sites having nearly half the radials blocked at the lowest elevation. Moreover, one or more beams at higher elevations are also blocked. Of the 58 radars that fit the aforementioned criteria, 46 are located within the CONUS and are marked with a red circle in Figure 6. The remaining 102 radars are also all affected by blockage to varying degrees, though many have maximum blockage under 5% for the lowest elevation scan. It is notable that every radar is blocked to some extent at the lowest elevation tilt. A correction algorithm to compensate for PBB would benefit the entire network, especially for the third that are more severely affected.

2.2 Current NEXRAD Blockage Mitigation

Within the ORPG computing environment, digital elevation maps (DEM), or terrain data, are available for algorithms to utilize to compensate for negatively biased reflectivity measurements. Currently, a correction factor is computed based on the beam height and blockage height for the hydrometeor classification algorithm (Park *et al.*, 2009) as well as for rain rate estimation algorithms. However, standard NEXRAD reflectivity and VIL products do not use any correction for reflectivity to compensate for PBB.

The correction is applied by estimating the amount of blockage, as a percentage, by

$$\alpha = 100\,\frac{\theta_b - \theta_s + \theta_{3dB}/2}{\theta_{3dB}}, \qquad (1)$$

where θ_b is the elevation angle of the beam, θ_s is the elevation angle of the blockage source, and $\theta_{3dB}$is the width of the beam. Then, a term known as F_{shield} is estimated as

$$F_{shield} = 0.5\tanh[0.0277(50-\alpha)] + 0.5, \qquad (2)$$

and is used to correct reflectivity as follows:

$$Z = Z_b - 10\log_{10}(F_{shield}), \qquad (3)$$

where Z_b is the raw reflectivity data in dBZ. The amount of bias correction applied using the F_{shield} parameter is shown in Figure 7. It can be seen from the figure that when no blockage exists, approximately 0.25 dB is added to the data when no correction is necessary. In order to prevent overcorrection in low blockage areas, a minimum blockage requirement of 5% should be used.

When correcting for blockage effects in rain rate estimation, the method is only applied if blockage is less than 70% as the technique is not reliable when the negative bias is greater than 6-8 dB. Other problems can occur when blockage sources vary depending on the season, such as deciduous trees, and can cause partial blockage at higher percentages in the spring and summer. Moreover, the available DEM only account for natural blockage and do not account for blockage due to man-made objects. Even if the DEM were updated regularly to reflect changes in the surroundings of the radar, they would only apply under standard beam propagation. Changes in the atmosphere can cause the beam to bend away or toward the earth, degrading the effectiveness of the algorithm. Dual polarization variables can be used instead to improve the negative bias due to PBB.

3. THEORY

The radar hardware upgrade to dual polarization brings new possibilities in correcting for PBB as differential phase, which is practically immune to partial blockage, can be used to estimate LWC in the atmosphere.

3.1 Z - Z_{DR} - K_{DP} Method

One algorithm leveraging the dual pol upgrade is based on the interdependency of reflectivity (Z), differential reflectivity (Z_{DR}), and specific differential phase (K_{DP}) in rain, which has been used to calibrate reflectivity (Ryzhkov *et al*., 2005). A correction factor for reflectivity for each radial is computed and added to the data in the radial, similar to the current, operational algorithm. The reasoning for correcting Z using interdependency is based on the fact that K_{DP} is immune to blockage. However, Z_{DR} can be affected by PBB so a simplified yet robust relation, not dependent on Z_{DR}, is used to mitigate the potential effects of bias on Z_{DR}.

A simple power law relation between K_{DP} and Z from Ryzhkov *et al*. (1997) is used in this method.

$$K_{DP} = aZ^b. \quad (4)$$

a is a variable intercept that is estimated from scan-to-scan from radials with no blockage. Using the radial integral of K_{DP} (i.e., Φ_{DP}) and Z^b, we can compute a ratio between the two for unblocked radials as

$$a = \frac{\int_{r_0}^{r_m} K_{DP(s)ds}}{\int_{r_0}^{r_m} Z^b(s)ds} = \frac{\Phi_{DP}(r_m) - \Phi_{DP}(r_0)}{2\int_{r_0}^{r_m} Z^b(s)ds}. \quad (5)$$

This ratio assumes reflectivity is well calibrated and not biased by attenuation. For radials where blockage is greater than a predetermined threshold, the ratio is computed as

$$a_B = \frac{\Phi_{DP}(r_m) - \Phi_{DP}(r_{0B})}{2\int_{r_{0B}}^{r_m} [(1-BBF)Z(s)]^b ds}. \quad (6)$$

BBF is the blockage percentage as a fraction, where 100% blockage is 1, and r_{0B} is the range to the first gate where blockage begins. The bias correction to be applied can then be computed as

$$\Delta Z(dB) = \frac{10}{b}\log\left(\frac{a_B}{a}\right). \quad (7)$$

A more detailed explanation of the algorithm can be found in Zhang *et al*. (2013).

The shortfalls of the algorithm are similar to the algorithm currently implemented on the WSR-88D. For the algorithm to run properly, the location of all blockage sources must be known, requiring the use of up-to-date DEM. As stated previously, some natural blockage sources change depending on the season and cannot be properly accounted for. Non-standard propagation of the beam also affects the algorithm as the correction is based on

knowledge of the proper location of blockage. Additionally, one of the parameters in the algorithm assumes homogeneity of drop size distribution and temperature within a given scan, which doesn't hold for various weather conditions. Reflectivity must also be corrected for attenuation.

3.2 Specific Attenuation Method

Due to some of the shortcomings of the algorithm, NSSL developed an improved algorithm to address these issues. Instead of correcting for reflectivity, LWC is computed directly from specific attenuation (A_h) and is then used to derive VIL from this measurement that is immune to blockage and miscalibration.

VIL is currently computed from reflectivity as

$$VIL = \int M(h)dh, \tag{8}$$

and is measured in kg/m^2 and h is derived from the vertical beam width. LWC is estimated as

$$M = 3.44 * 10^{-3} Z^{\frac{4}{7}}, \tag{9}$$

where M is measured in g/m^3 and Z is in mm^6 m^{-3}.

Simulations on drop size distributions from Oklahoma suggest a new estimate for M as

$$M = a(t){A_h}^{0.93}, \tag{10}$$

where $a(t)$ is a temperature dependent term defined as

$$a(t) = 70.8 + 2.04t + 0.21t^2, \tag{11}$$

where t is measured in Celsius. Currently, a linear vertical profile of temperature is used to simulate the temperature change in height relative to the melting layer.

Specific attenuation is obtained parametrically for each range bin along a radial from Z and Φ_{DP} as

$$A_h = \frac{Z^b(r) * \{10^{0.1b\gamma\Delta\Phi} - 1\}}{I(r_1, r_0) + \{10^{0.1b\gamma\Delta\Phi} - 1\} I(r, r_0)}, \tag{12}$$

and is expressed in dB/km. $I(r, r_0)$ is defined as

$$I(r, r_0) = 0.46b \int_r^{r_0} Z^b(s)ds. \tag{13}$$

b is constant at S band and is determined to be 0.72 through simulations by disdrometer data in Oklahoma (Ryzhkov *et al*., 1997) and γ is 2.88 x 10^{-2} at S band (Testud *et al*., 2000).

In the current implementation of the algorithm, an assumption is made that the entire tilt is composed of liquid when estimating the LWC, even above the melting layer. This is consistent with the operational reflectivity based VIL estimation. A correction can be applied to account for melting layer contamination but the assumption of liquid water is still made. The radar has the ability to distinguish between liquid and frozen hydrometeors using the hydrometeor classification algorithm. In future work, other relations using dual pol measurements for frozen hydrometeors should be explored for a more accurate estimate of VIL.

4. PRELIMINARY RESULT

The Tucson, AZ NEXRAD site is located in the Santa Rita Foothills and is surrounded by mountain ranges. Figure 8 shows the blockage map for the 0.5° tilt, one of several affected by terrain up through 4.0°. In the areas outside the completely blocked (bright red) radials, an improvement in the estimation of LWC is expected for each tilt. Currently, where the beam is partially blocked, Z is negatively biased resulting in VIL values lower than expected for a weather event. The perceived potential severity of a convective storm is lessened due to this bias. The amount of VIL reduction for any given storm is a function of a) storm dynamics, and b) relationship of storm range from the radar, volume coverage pattern, and amount of partial blockage.

Figure 9 shows a side-by-side comparison of VIL where LWC is computed using Z and A_h.The left image shows VIL for the entire volume using the LWC relation for Z and is what is incorporated into mosaics used by the FAA automated weather

systems. On the right is VIL using the relation for A_h. To the north and northwest of the radar, the visible increase in VIL can easily be seen where blockages range from 0-90% (recall Figure 8). However, to the southeast of the radar, there is a decrease in VIL when compared to the Z method. This finding needs further understanding and will be resolved as the algorithm is further developed.

There are several advantages of using specific attenuation to compute LWC as defined in (10). Foremost is that standard reflectivity and VIL products from NEXRAD have no PBB mitigation. A further advantage is that unlike the current version of blockage correction, this method corrects for partial blockage while being robust to radar miscalibration. Ryzhkov *et al*. (2013) also show that the LWC relation using specific attenuation is more robust to variations in drop size distributions when compared to the relation using reflectivity. Another important advantage is no prior knowledge of the location of blockage is necessary for the algorithm to function if the blockage is close to the radar and the blockage percentage does not change along a radial. Unlike the correction methods based on (3) and (7), which require knowledge of blockage location, the algorithm is robust enough that seasonal variations in blockage would not affect the function of the algorithm as blockage need not be known. Similarly, if the propagation of the beam changes due to atmospheric conditions, the algorithm should not be affected given that a proper temperature profile is utilized.

While the results are certainly encouraging, there are some tradeoffs to consider. Currently, dual pol variables are only available to 300 km while reflectivity and VIL have a limit of 460 km. Discontinuities at 300 km will arise due to this difference and the algorithm will need to be modified to properly transition between the two regions.

The estimate of $M(A_h)$ is also prone to variability of the A_h/K_{DP} ratio as drop size distributions can have an effect on the ratio (Ryzhkov *et al*., 2013). However, the variability of A_h/K_{DP} due to drop size distributions is less than the variability in $M(Z)$.

The LWC relation with reflectivity can be biased due to changes in drop size distribution but is not influenced by temperature whereas the relation with specific attenuation is sensitive to temperature. This can be mitigated through the use of model data. The ORPG algorithm environment has the additional capability of accessing model data. Hallowell *et al*., (2013) use model data in the ORPG to determine multiple freezing level heights for each grid point. A similar method could be used to provide a more accurate vertical temperature profile for each grid point over the radar domain for the correction algorithm every hour instead of relying on knowledge of the height of the melting layer and using a linear vertical profile for temperature.

As the algorithm is further developed, a method to compare performance against the current VIL algorithm will be required. The mosaics currently used in FAA weather systems will be considered the “standard” to compare against. Mosaics will be created using VIL corrected for PBB and compared to the current mosaic to determine the level of benefit the correction has. The expectation is to improve the quality of the product in areas where blockage exists while not affecting the accuracy elsewhere.

5. SUMMARY

The accurate depiction of weather is a very important issue for flight controllers for safe and efficient management of air traffic. The current version of VIL serves controllers well. The upgrade of the WSR-88D radars to dual polarization allows for another improvement to the fidelity conveyed of the actual state of the atmosphere in areas of PBB.

A description and preliminary results of a new algorithm to compute VIL has been presented and compared to the traditional VIL algorithm. There is promise in the algorithm to further improve the data quality of VIL used by automated weather

systems. Some tradeoffs must be considered when using this algorithm but the potential benefits to recover VIL in areas of PBB, as illustrated earlier, and the robustness to radar miscalibration cannot be overlooked. Using Φ_{DP} with the attenuation technique with model data, there is potential to further improve the algorithm to more accurately estimate VIL.

6. REFERENCES

Evans, J.E. and E.R. Ducot, 2006: Corridor Integrated Weather System. *MIT Lincoln Laboratory Journal*, **16**, 59-80.

Evans, J.E. and E.R. Ducot, 1994: The Integrated Terminal Weather System (ITWS). *MIT Lincoln Laboratory Journal*, **7**, 449-474.

Federal Aviation Administration website, (August 2013): Passenger Boarding (Enplanement) and All-Cargo Data for U.S. Airports. Retrieved from http://www.faa.gov/airports/planning_capacity/passenger_allcargo_stats/passenger/.

Green, D.R., and R.A. Clark, 1972: Vertically integrated liquid water – A new analysis tool. *Mon. Wea. Rev.*, **100**, 548-552.

Hallowell, R.G., M.F. Donovan, D.J. Smalley, and B.J. Bennett, 2013: Icing hazard detection with NEXRAD IHL. *Proc. American Meteorological Society's 36th International Radar Conference, Breckenridge, CO.*

Park, H., A.V. Ryzhkov, D.S. Zrnic, and K-E. Kim, 2009: The hydrometeor classification algorithm for the polarimetric WSR-88D: Description and application to an MCS. *Wea. Forecasting*, **24**, 730-748.

Ryzhkov, A.V., D.S. Zrnic, and D. Atlas, 1997: Polarimetrically tuned R(Z) relations and comparison of radar rainfall methods. *Jour. Appl. Meteor.*, **36**, 340-349.

Ryzhkov, A.V., S.E. Giangrande, V.M. Melnikov, and T. J. Schuur, 2005: Calibration issues of dual-polarization radar measurements. *J. Atmos. Oceanic Technol.*, **22**, 1138-1155.

Ryzhkov, A., M. Diederich, P. Zhang, and C. Simmer, 2013: Potential utilization of specific attenuation for rainfall estimation, mitigation of partial beam blockage, and radar networking. Submitted to *J. Atmos. Oceanic Technol*.

Smalley, D.J. and B.J. Bennett, 2002: Using ORPG to enhance NEXRAD products to support FAA critical systems. *10th Conference on Aviation, Range, and Aerospace Meteorology (ARAM)*, Portland, OR, Amer. Meteor. Soc.

Smalley, D.J., B.J. Bennett, and M.L. Pawlak, 2003: New product for the NEXRAD ORPG to support FAA critical systems. *19th Conference on Interactive Info Processing Systems in Meteorology, Oceanography, and Hydrology (IIPS)*, Long Beach, CA, Amer. Meteor. Soc.

Testud, J., E. Le Bouar, E. Obligis, and M. Ali-Mehenni, 2000: The rain profiling algorithm applied to polarimetric weather radar. *J. Atmos. Oceanic Technol*., **17**, 332-356.

Williams, E., K. Hood, D. Smalley, M. Donovan, V. Melnikov, D. Forsyth, D. Zrnic, D. Burgess, M. Douglas, J. Sandifer, D. Saxion, O. Boydstun, A. Heck, T. Webster, 2013: End-to-end calibration of NEXRAD differential reflectivity with metal spheres. *Proc. American Meteorological Society's 36th International Radar Conference, Breckenridge, CO.*

Zhang, P., D. Zrnic, and A. Ryzhkov, 2013: Partial beam blockage correction using polarimetric radar measurements. *J. Atmos. Oceanic Technol.*, **30**, 861-872.

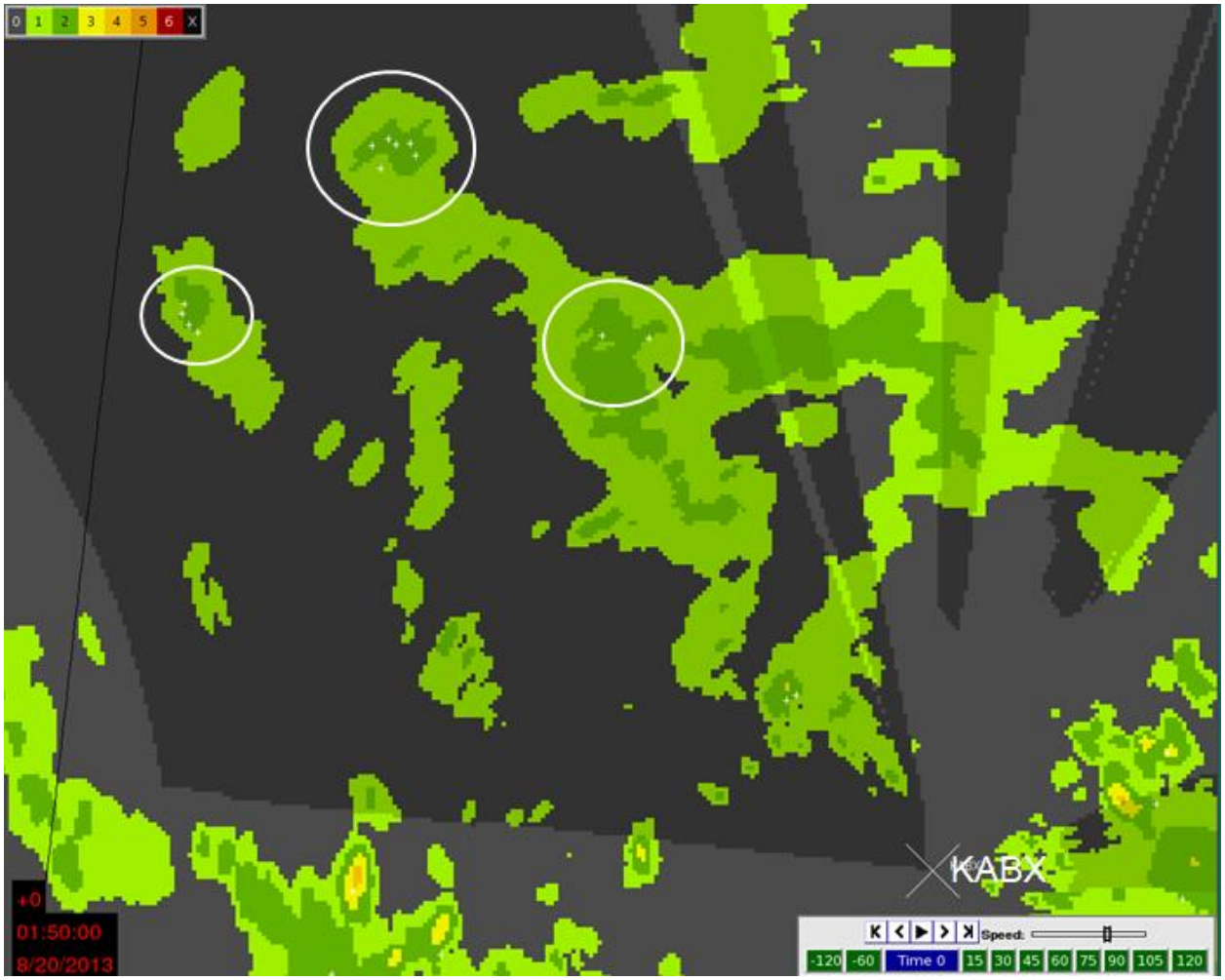

Figure 1. CIWS VIL mosaic northwest of the KABX (Albuquerque, NM) radar on August 20, 2013 at 0150 Z. The darker colors indicate where only far range and beam blocked radar data are available. Within the white circles, the VIL is likely under reported due to KABX PBB. The VIL precipitation only shows level 1 and 2 returns where lightning indicated by the small white crosses are present. The KABX echo top returns showed 30 and 35 kft 18 dBZ echo top values at these locations. Higher echo top values and lightning could be an indicator of more severe weather not indicated in VIL due to PBB.

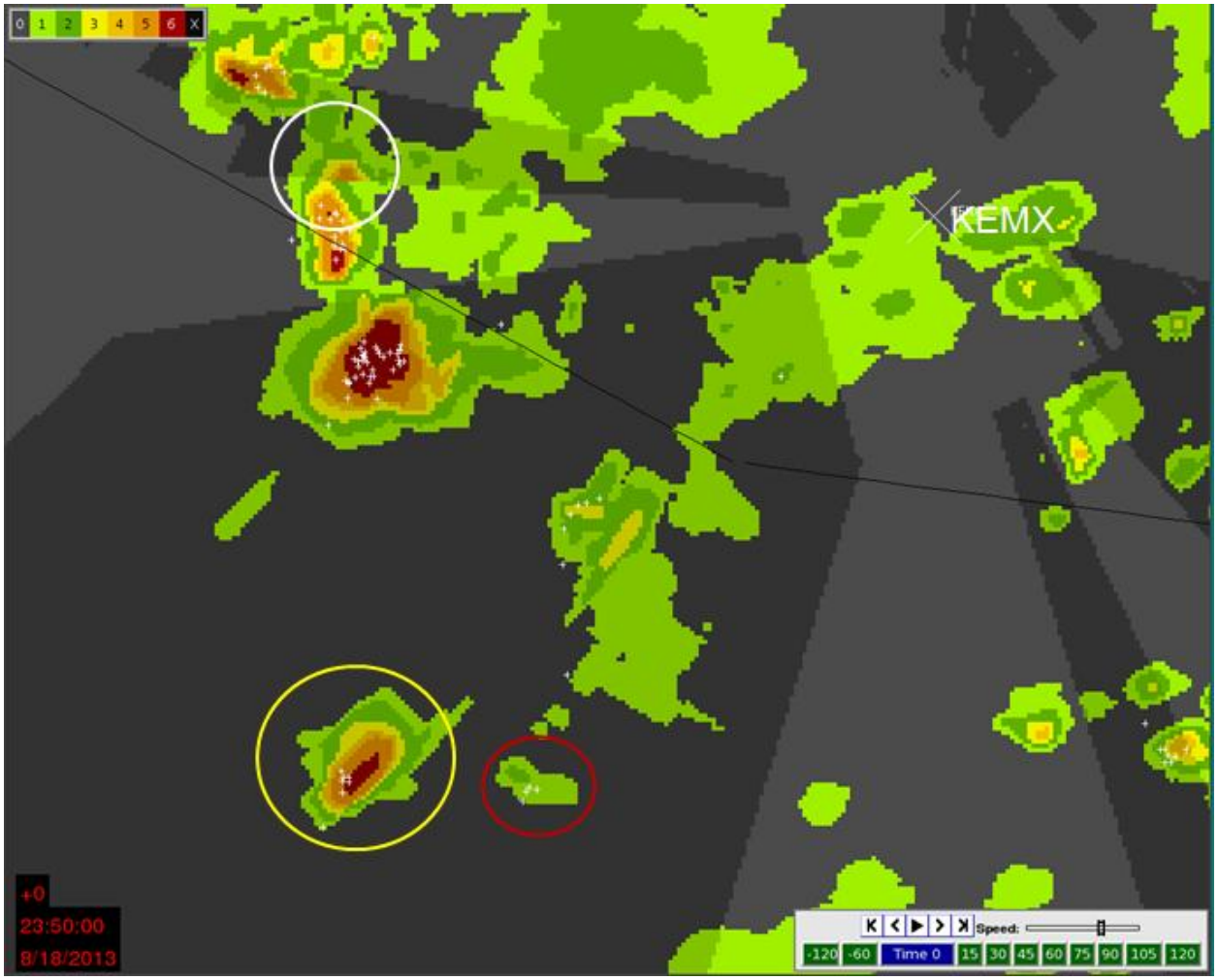

Figure 2. CIWS VIL mosaic artifacts due to beam blockage on August 18, 2013 at 2350 Z south of KEMX (Tuscon AZ). The dark gray background shows where all radars are either far range or beam blocked. In this image, beam blockage in the KEMX radar and KIWA (Phoenix, AZ) radar to the north cause several types of artifacts in the CIWS VIL mosaic. Within the white circle there is a discontinuity across an area where the KEMX data is the only near radar considered not to be beam blocked. KEMX data is used exclusively by the mosaic in that location and where KEMX is flagged as possibly being affected by beam blockage (dark gray background), the mosaic strategy switches to using the highest radar data overall. This logic selects data from a radar further away, thus displaying the storm as more spread out and in a slightly different location. The storm in the yellow circle is from the KYUX (Yuma, AZ) radar located further away to the west. That cell is not present in KEMX VIL or Echo Top outputs as the KEMX beam blockage is more severe in those radials at lower elevations. The cell in the red circle originating from the KEMX VIL is likely underestimated as lightning is present but only level 1 and 2 precipitation are shown.

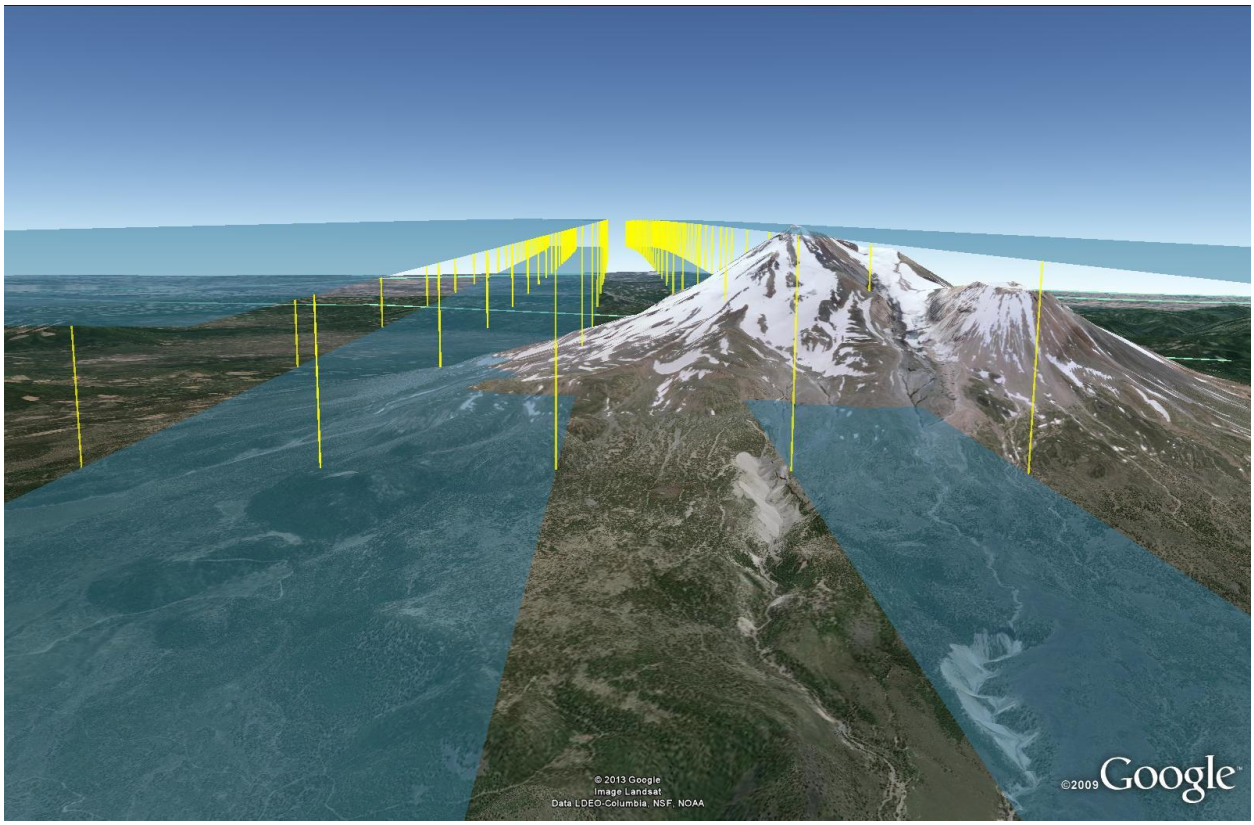

Figure 3. Natural blockage to the southeast of the KMAX Medford, Oregon NEXRAD. Mt. Shasta can be seen partially blocking the beam for several azimuth angles. Three azimuths are shown in this figure: the 147° radial with no blockage on the far left, the 148° radial with minor blockage, and the 150° radial with near complete blockage. The radar is in the reader's position. (Google and the Google logo are registered trademarks of Google Inc., used with permission.)

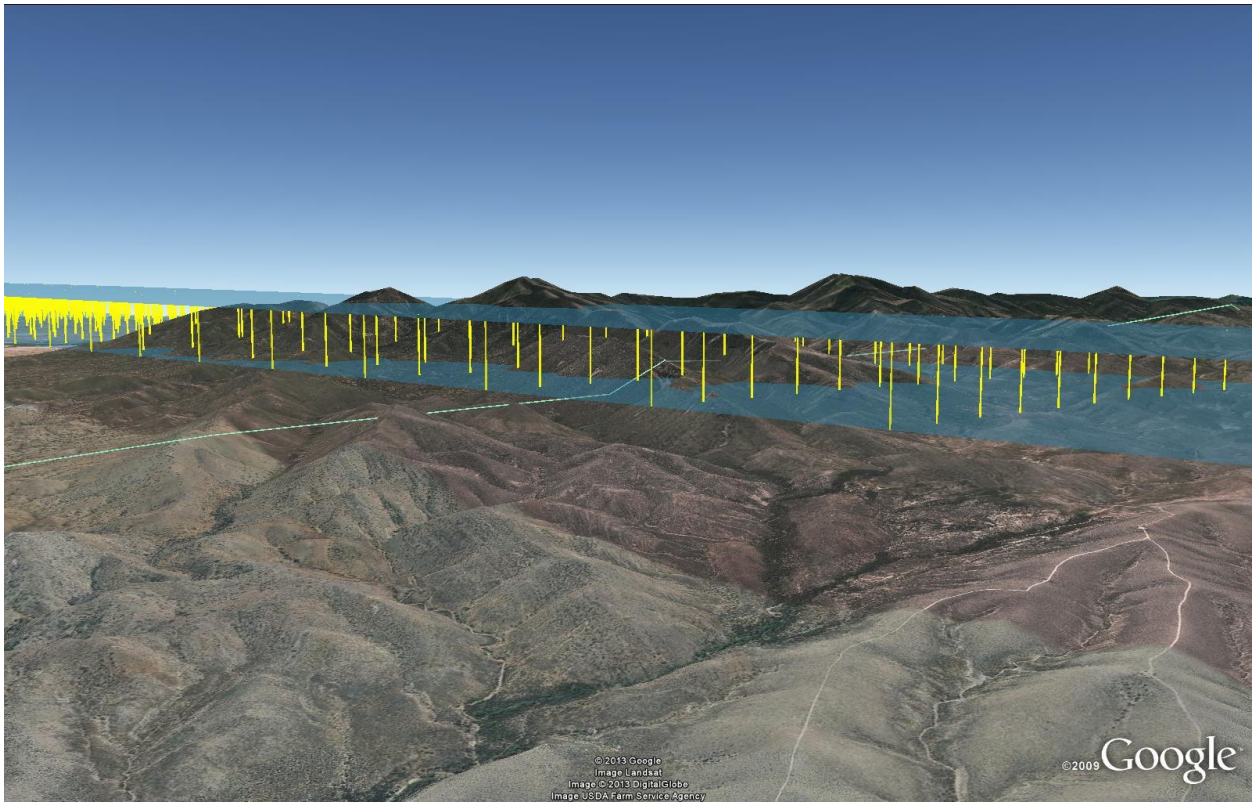

Figure 4. Natural blockage to the east of the KEMX Tucson, Arizona NEXRAD. A lower level of blockage can be seen at the right of the image with blockage percentage increasing as the beam propagates out in range. The radar is to the right of the page. (Google and the Google logo are registered trademarks of Google Inc., used with permission.)

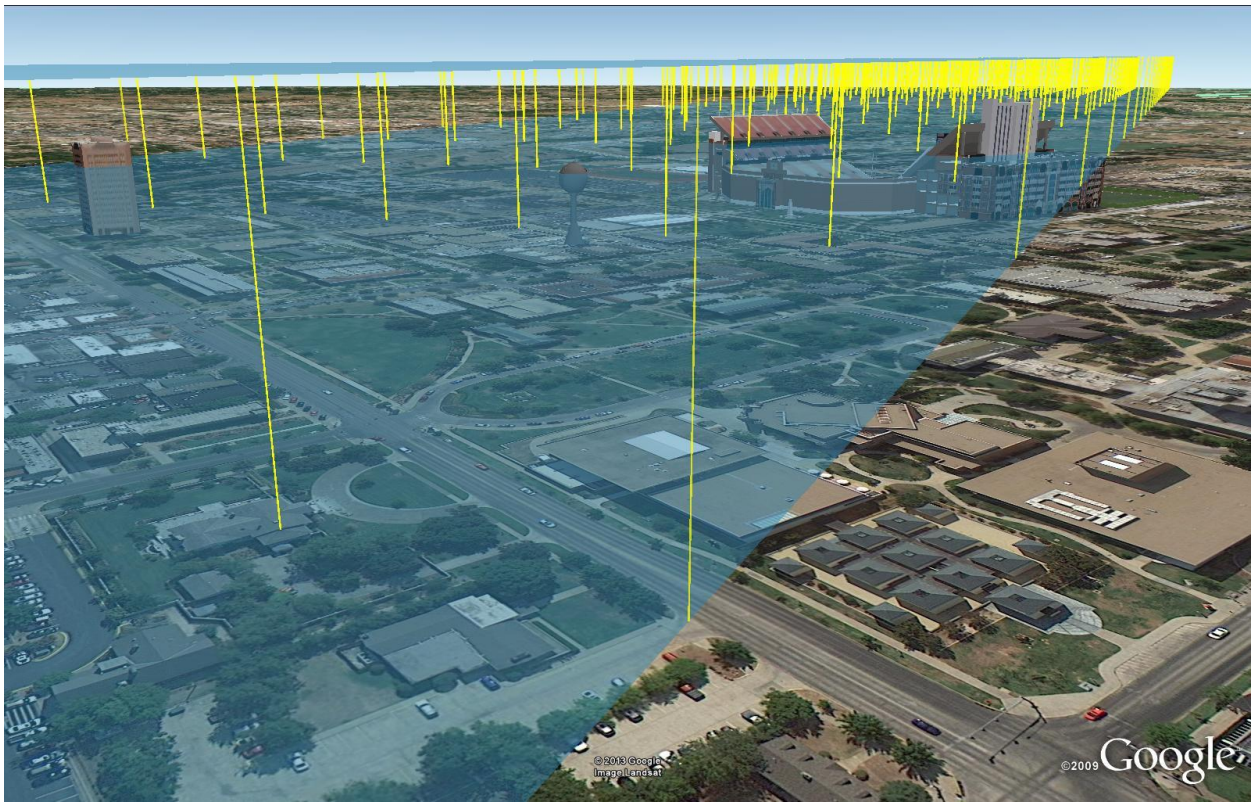

Figure 5. Man-made blockage to the southeast of the KOUN Norman, Oklahoma research radar. Various structures on the campus of the University of Oklahoma partially block the beam. The radar is to the lower left of the image. (Google and the Google logo are registered trademarks of Google Inc., used with permission.)

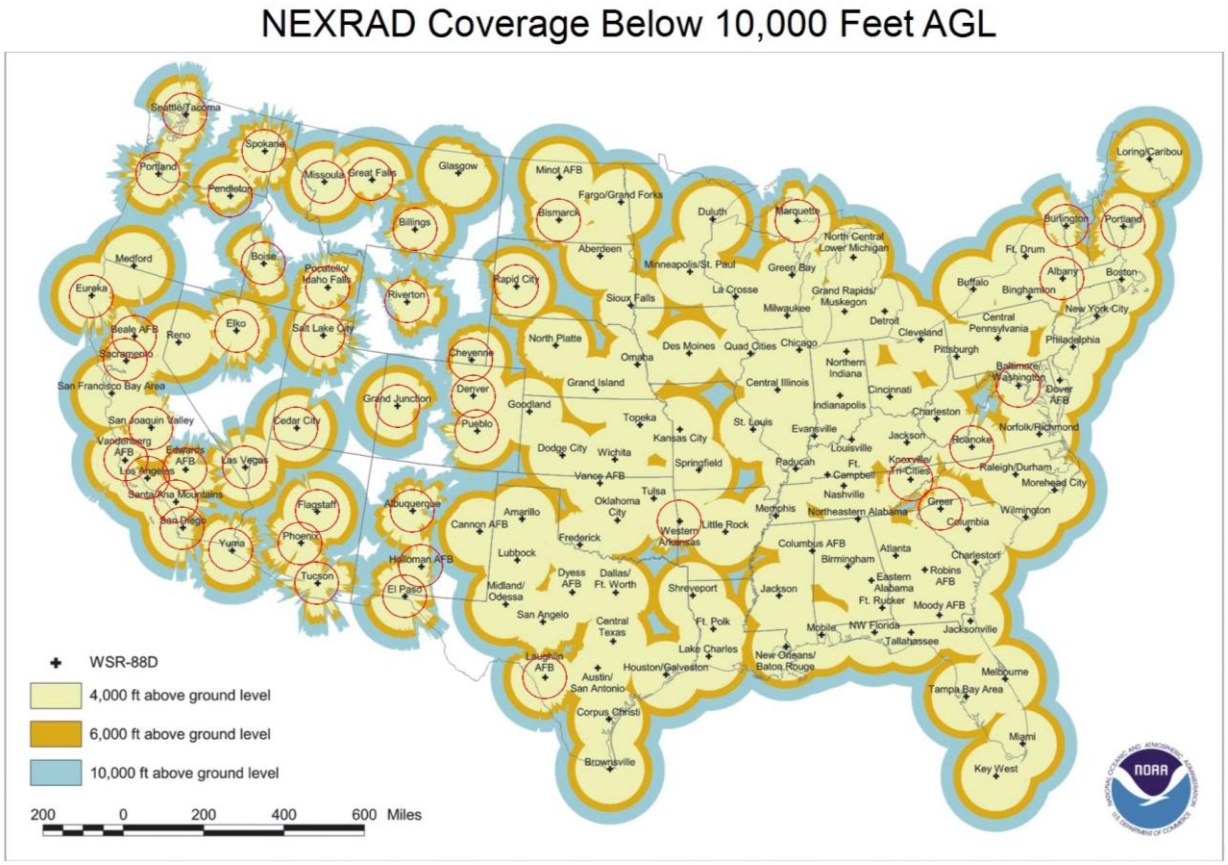

Figure 6. NEXRAD coverage for various altitudes above ground level in 2000. Radars marked in red denote at least 50% blockage in a minimum of 10% of the radials at the lowest elevation tilt. (Courtesy of SRI International)

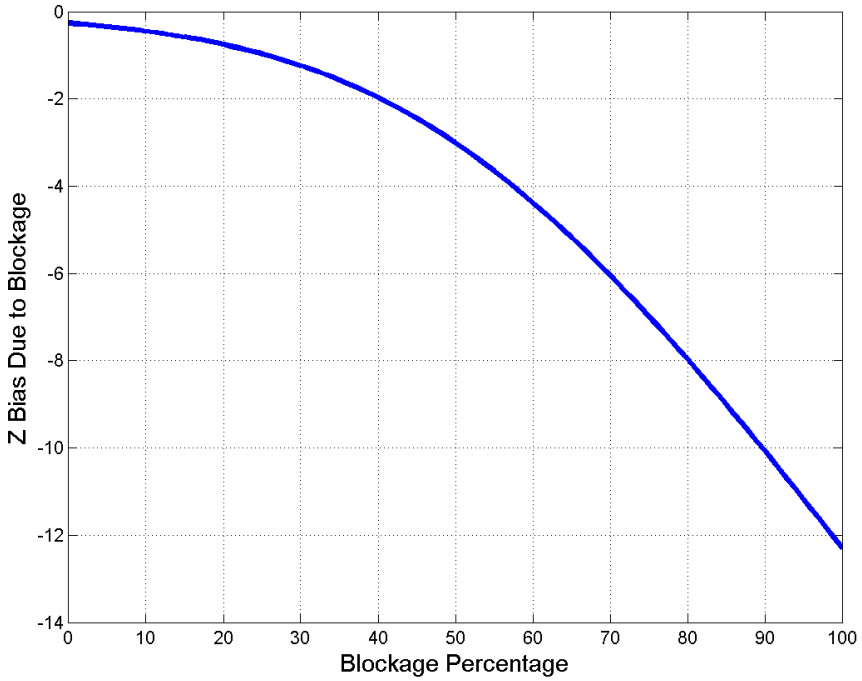

Figure 7. Plot of the bias in *Z* due to blockage using (2). A minimum threshold of 5% blockage should be used to prevent overcorrection in areas of low beam blockage. In algorithms utilizing the F_{shield} parameter, corrections are not made when blockage is greater than 70%.

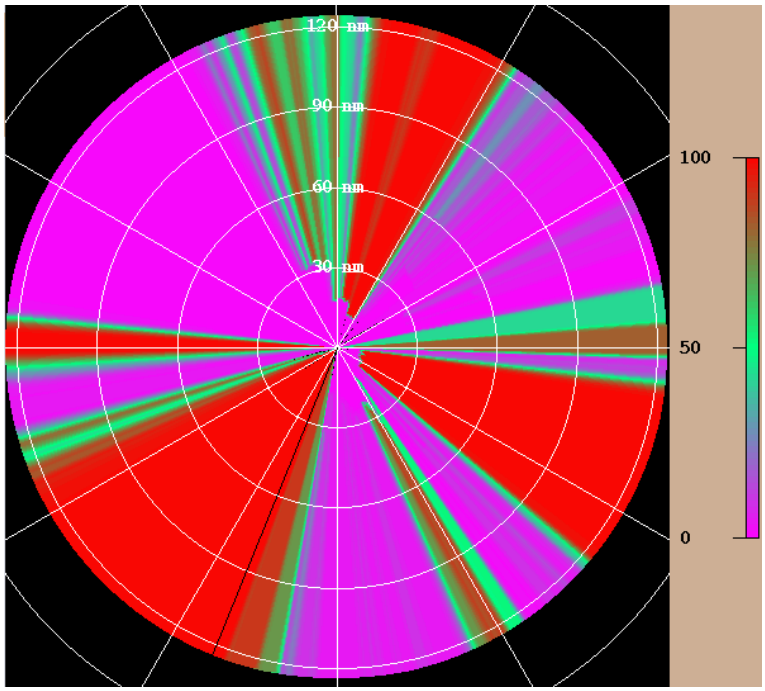

Figure 8. Blockage map for KEMX (Tucson, AZ) radar site at 0.5° elevation. Complete blockage and no blockage are represented as bright red and purple, respectively. Improvements to VIL should be apparent in areas that are not completely blocked (green to dark red) by the mountains.

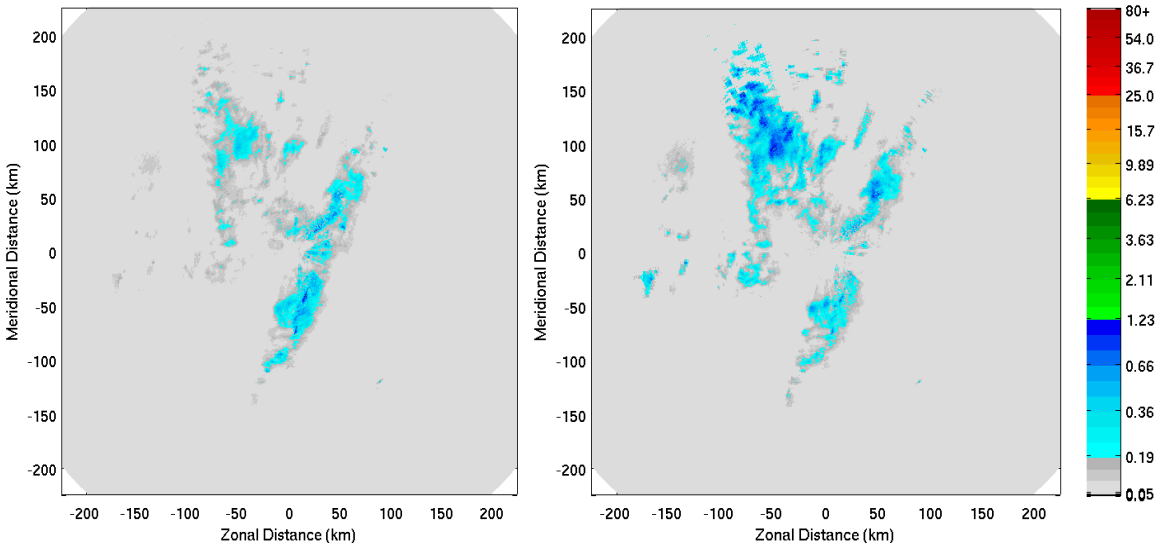

Figure 9. VIL images from the Tucson KEMX radar on March 18, 2012 at 1615Z. VIL as currently estimated using only reflectivity is on the left while VIL computed using dual pol measurements is on the right. Recovery of VIL in areas of PBB can be clearly seen to the northwest of the radar.